A Flood Prediction Benchmark Focused on Unknown Extreme Events

Dimitri Bratzel, Stefan Wittek and Andreas Rausch
Institute for Software and Systems Engineering, Clausthal University of Technology,
Arnold-Sommerfeld-Str. 1, Clausthal-Zellerfeld, Germany

Keywords: Machine Learning, Flood Prediction, Benchmark, Dataset, Unknown Events.

Abstract: Global warming is causing an increase in extreme weather events, making flood events more likely. In order to prevent casualties and damages in urban areas, flood prediction has become an essential task. While machine learning methods have shown promising results in this task, they face challenges when predicting events that fall outside the range of their training data. Since climate change is also impacting the intensity of rare events (i.e. by heavy rainfall) this challenge gets more and more pressing. Thus, this paper presents a benchmark for the evaluation of machine learning-based flood prediction for such rare, extreme events that exceed known maxima. The benchmark includes a real-world dataset, the implementation of a reference model, and an evaluation framework that is especially suited analysing potential danger during an extreme event and measuring overall performance. The dataset, the code of the evaluation framework, and the reference models are publicated alongside this paper.

1 INTRODUCTION

Global warming not only leads to a rise in temperature but also causes an increase in the frequency and intensity of extreme weather events. Floods are one such example of an event affected by this trend (Alfieri et al., 2017).

In order to mitigate the negative impact of floods, accurate and timely predictions of flood events are critical. Predictions made 2-3 hours in advance can provide crucial warning time to allow evacuation and the implementation of preventative measures, thereby reducing the damage caused by floods.

Artificial neural networks (ANN) and other machine learning (ML) methods have shown promising results in the prediction of flood events (Goymann et al., 2019). However, a major challenge in flood prediction is the issue of unknown extreme events. If the precipation or the resulting water levels exceed previous records, the ML algorithm is forced to extrapolate – i.e., to do predictions outside of the range of its training data. Many ML algorithms, especially ANN, are known to perform poorly in extrapolation scenarios (Minns and Hall, 1996). Another factor that complicates unknown extreme events is the rare occurrence of even the known extreme events in the training set. This makes predictions even more challenging.

These challenges are becoming increasingly relevant with the effects of climate change, which are likely to lead to an increase in the frequency of record-breaking heavy rain and, consequently floods in the future.

Despite the importance of this issue, existing works on the extrapolation of ML-based flood predictions are limited, with most studies focusing on performance within the range of the training data. While public datasets on water levels exist, they are missing a framework for actual comprehensive evaluation as well as a focus on unknown events and extrapolation.

In this paper, we provide a benchmark based on the city of Goslar in Germany, focusing on the aforementioned challenges in flood predictions. This benchmark case is particularly important since it is located near the Harz region, a mountainous area in Lower Saxony. Areas like this are suspected of suffering from this increase in flood events as a result of global warming (Allamano et al., 2009).

This benchmark includes the real-world dataset spanning about 14 years and including one big flood event as well as an evaluation framework focused on the performance of these unknown situations. We

Bratzel, D., Wittek, S. and Rausch, A.
A Flood Prediction Benchmark Focused on Unknown Extreme Events.
DOI: 10.5220/0012081700003546
In *Proceedings of the 13th International Conference on Simulation and Modeling Methodologies, Technologies and Applications (SIMULTECH 2023)*, pages 267-278
ISBN: 978-989-758-668-2; ISSN: 2184-2841

also provide a reference implementation using a Long-Short-Term-Memory (LSTM) model. For the evaluation framework as well as for the reference implementation, code is provided[1].

This allows other researchers to test their ML-based flood prediction approaches with respect to unknown events and compare the performance with our baseline implementation.

The paper is structured as follows. After stating the related work in section 2, section 3 gives a detailed description of the data set. Section 4 describes the predictiv task definded based on this dataset. Section 5 contains the evaluation framework, incuding an event focused framework (section 5.1) and a variety of metrics applied to the overall prediction quality (section 5.2). In section 6 a reference precitive model is described which is evaluated using the framework in section 7.

2 RELATED WORKS

The discussed related work in this section can be separated as follows: The forecast of a flood event through ML, dealing with unseen events, datasets, and mainly used framework for evaluating hydrological models.

The ML-Based Flood Prediction

An extensive range of research has been done on forecasting a high-water event. Usually, these papers differ in hydrogeological features or the ML-technology that was used to forecast the flood event. This leads to the differences in the range of the forecasting window, the data quality and quantity, and the event that needs to be forecasted. Since ANN offers advantages such as rapid development, low execution time, the parsimony of data requirements and a substantial open-source community (Shamseldin, 2010), many works are using this technique. Riad et al. discuss the forecast of a flood event with a one-layer artificial neural network on data collected in the Ourika basin in Morocco from 1990-1996 (Riad et al., 2004). Shameseldin et al. apply the Multi-Layer Perceptron (MLP) model for the Nile River in Sudan. The model considers data such as rainfall index and seasonal expectation rainfall index, and other meteorological input information (Shamseldin, 2010). A similar application of MLP was used in the region of Greater Manchester, where the application of MLP was justified because this technique is more suitable for finding patterns and trends in complex data than regular statistical models and algorithms (Danso-Amoako et al., 2012). Although Danso-Amoako et al., in their work, do not forecast the future status of water level or similar, they predict the actual risk of dam failure by creating a data-driven surrogate model with using a MLP model. Very different is the case in catchments with open water, for example, coastal areas, where different sources may cause the occurrence of extreme storm surges. In their work Kim et al. discuss these effects of the surge and test them on a MLP model to predict the surge in the coastal region of Japan in Tottori (Kim et al., 2016). Although the results are promising, the target of the forecast is so-called "after-runner surge”, which occurs 15-18 hours after a typhoon. Therefore, two important pieces of information are used for the forecast: the quantitative description of the typhoon and the knowledge that an extreme surge event is very likely to occur within the next 18 hours. A comparison of the performance of different techniques: MLP, Adaptive Neuro-Fuzzy Inference System (ANFIS) and empirical models, on a huge area of Peninsular Spain is presented in (Jimeno-Sáez et al., 2017). A good systematic overview of the ML-based prediction was done in (Mosavi et al., 2018) where most common ML techniques are explained and their application in different areas datasets and forecast horizons are presented.

Prediction of Extreme Events

Despite the good results in forecasting weather phenomena, most of the works deal with problems in finding a pattern and recognizing an event that has already happened in the past. The anomalous behaviour of Artificial Neural Networks on forecasting unseen events was observed in (Minns and Hall, 1996), where the ANN performed very well on test data that had the same minimal and maximal values but could not overcome the maximal values in the test set where the flood event had higher values than the ones that could be observed on training data. The authors concluded that MLP tends to recall seen values but has problems generalizing if the flood event shows higher values than the training data. To solve the problem in (Hettiarachchi et al., 2005), the solution of the so-called Estimated Maximum Flood (EMF) was presented. In this case, the authors used additional domain knowledge to generate artificial data where an extreme event appears. This extreme event is much higher than ever observed empirical data with a probability higher than zero. The problem was also observed and discussed in (Xu et al., 2020)

[1] https://gitlab.com/tuc-isse/public/flood-benchmark

where the general problem of extrapolation of ANN was analysed and theoretical and empirical evidences were given that simple ANN does not predict properly when values are out of the range of the training sample. Whereas (Pektas and Cigizoglu, 2017) observe the ANN behaviour in the hydrology during minima and maxima of the dataset that are out of the training sample. (Goymann et al., 2019) presented in their work in the catchment Goslar the forecast of the flood event from 2017. Facing a similar problem with LSTM-ANN, the authors provided a classification-based approach. Therefore, the result was a value of one if it was expectable that a flood event in the next two hours could appear or zero if no flood event was expected.

Flood Prediction Metrics

To evaluate the prediction models, several metrics were used. This includes well-known, mean-based metrics like root mean squared error (RMSE) (Dtissibe et al., 2020; Jimeno-Sáez et al., 2017; Mulualem and Liou, 2020), normalized root mean square error (NRMSE) (Kim et al., 2016), mean absolute and relative error (MARE) (Dtissibe et al., 2020; Riad et al., 2004) also indices like the correlation coefficient (CC) (Kim et al., 2016) and coefficient of determination (R^2) (Danso-Amoako et al., 2012; Jimeno-Sáez et al., 2017; Riad et al., 2004; Shamseldin, 2010). The main disadvantage of mean-based metrics is that even significant forecast errors decrease with the increasing number of right-predicted values. This is a problem in big datasets where an extreme, rare event should be predicted. The paper (Krause et al., 2005) discusses several efficiency criteria for the hydrological model. The leading critique is that the Nash-Sutcliffe efficiency (NSE) and the index of agreement (IoA) are sensitive to errors in the peaks and less sensitive to systematic errors in lower regions. By modifying the metrics, authors propose how these metrics could be used as a benchmark to evaluate errors in lower and higher regions.

During the research, no related work could be found that could fulfil the requirements for the application in the catchment area of Goslar for the forecast of values during high water levels, such as: show difference of prediction versus Ground Truth, robustness against growing number of predicted values, explanation of errors (systematic error or outlier), exact focus on the performance during critical time (flood event).

Therefore, we present a benchmark that includes the dataset of a rare extreme flood event, an evaluation framework with event-focused evaluation framework and modified overall metrics and the example of the application of residual LSTM-Neural Network on the problem of flood forecast in 2, 3 and 4 hours.

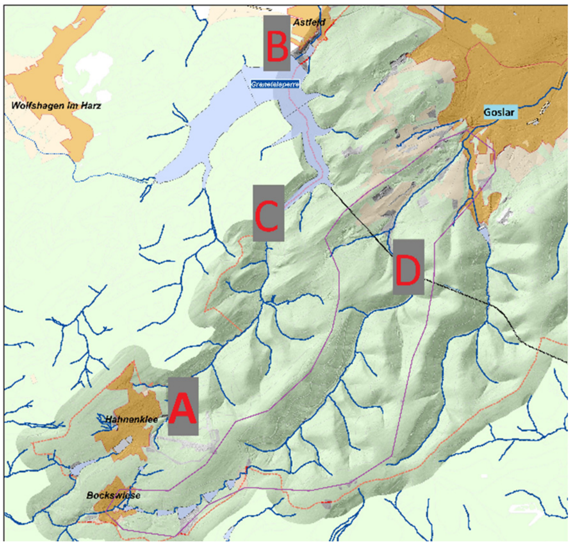

Figure 1: Geological overview of catchment Goslar (City Goslar, Goymann, et al. 2019).

3 GOSLAR REGION DATASET

The catchment area of interest is the city of Goslar and the high ground part from the settlement in south-west (Figure 1). The river “Gose” (highlighted in purple) that was responsible for the flood event in 2017 could be measured at station Sennhuette (**D**) since the artificial under-earth connection between the dam “Granetalsperre” at (**B**) and the river Gose at Sennhuette (**D**) needs to be considered. As additional input for the sudden rainfall, the weather stations (**A**) Hahnenklee and (**B**) Margaretenklippe are available.

The river stream goes from the Southwest to the city in the Northeast; therefore, the sensors are essential to catch early data for sensing actual level of the Gose, that enter the city centre at (**D**), the latest point for measuring the water level before the city.

Granetalsperre (**C**) and Sennhuette (**D**) measure the actual level of the water in [cm]. The current of the water stream in [m^3/s], which is also part of the collected data, is not measured directly but is automatically derived from this level and mixed formal and parametrical model from Harzwasserwerke GmbH during data collection. The weather stations collect the rainfall in [l/m^2]. The data collection of all sensors happens every 15 minutes.

Table 1: Statistical overview of collected data.

	Granetalsperre [l/m²]	Hahnenklee [l/m²]	Margarethenklippe [cm]	Margarethenklippe [m³/s]	Sennhuette [cm]	Sennhuette [m²/s]
count	514176	514176	514176	514176	514176	514176
mean	0.03	0.04	10.40	0.12	7.98	0.11
std	0.19	0.21	5.84	0.20	6.26	0.20
min	0.00	0.00	3.70	0.01	1.50	0.01
25%	0.00	0.00	6.60	0.04	4.00	0.03
50%	0.00	0.00	8.70	0.07	6.00	0.05
75%	0.00	0.00	12.10	0.13	9.80	0.12
max	25.40	24.50	160.60	12.50	170.40	16.68

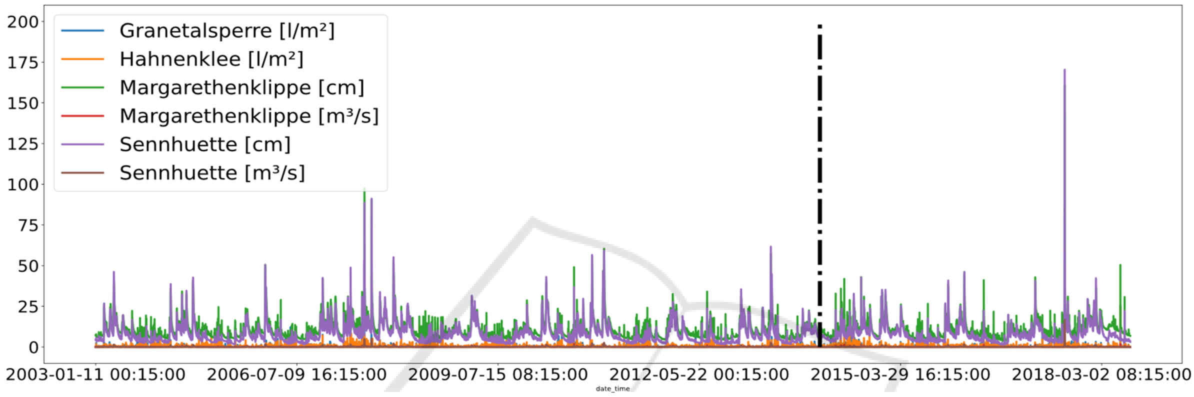

Figure 2: Split in training and test data.

The data set consists of 514176 samples in the time range from 01.11.2003 until 30.06.2018. In the statistical description (Table 1), it can be observed that the Sennhuette reaches its maximum value at 170.4 [cm], whereas the upper quartile is 9.8[cm]. This can be explained by the dataset that includes the flood event from 2017 in Goslar (Figure 3).

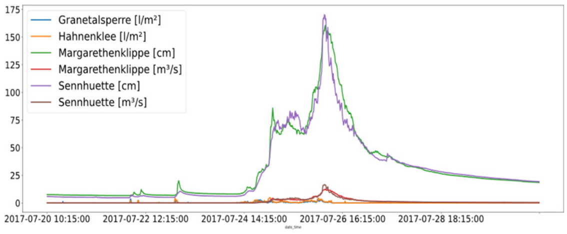

Figure 3: Data during flood event 2017, Goslar.

Thus, a similar effect can also be observed in the other data but the rainfall, where 75% of the data is 0. The situation where quartiles are very close to each other but relatively far away from the maximum value and the maximum value cannot be considered as an outlier; we call extreme, rare event. In the case of Sennhuette the maximal value is almost 17 times bigger than the upper quartile and cannot be reduced as an outlier since this is the actual value that needs to be predicted properly.

4 PREDICTIVE TASK

The hydrogeological experts of the catchment of Goslar agree that with the view on the growing importance of global climatic changes, the prediction of high-level water events will grow, since the risk of unexpected and intense rainfalls will grow. To allow emergency services to activate the protection procedure and warn the population of the catchment, a prediction of at least 120 minutes is required. Moreover, emergency services ask for immense forecast horizons like 180 minutes (3 hours) and 240 minutes (4 hours).

Even though previous work of the Institute of System Engineering at the Technical University of Clausthal shows a promising and robust forecast for the warning of extreme events that could meet the requirements (Goymann et al., 2019), show that despite accurate predictions of the water level, ANNs work poorly during an extreme event. Although the poor performance of regular ANN on unseen, rare events is known, no dataset could be found that represents the problem correctly. Therefore, the discussion about the evaluation of the performance of models to forecast extreme, rare, and unseen events could not make progress, which is demanded by global climatic changes and concepts of safety concerns.

For the training, 70% of the data can be used and 30% for testing. Even though more data could be used for predicting the extreme event, it must be considered that the extreme event must be a part of the test set (Figure 2) and operations like shuffling are only allowed to do after the split operation.

Therefore, the contribution of this work is a benchmark for predictive models containing the data set from the catchment area of Goslar including one extreme event, an event-focused evaluation framework and a set of adapted overall metrics.

The data, source code of the evaluation framework and reference implementations of models for 2-, 3- and 4-hours forecast are available as a git repository: https://gitlab.com/tuc-isse/public/flood-benchmark.

5 EVALUATION FRAMEWORK

The presented evaluation framework consists of an event-focused evaluation framework and a set of overall metrics suitable for evaluating the models. The event-focused part gives an insight on the performance of the model if applied to events that exceed this training horizon. In contrast the overall metrics allow the assessment of the model in general, without this focus.

5.1 Event-Focused Framework

As discussed in previous chapters, a sudden high-water event causes serious danger to the environment of the catchment. Also, we discussed how average-based metrics underestimate errors in regions with lower values. Therefore, a framework for evaluating predictive models was created that defines potential danger events and allows the framework to be adjusted to local hydrogeological conditions and safety concerns.

The schematic visualization of the event-focused framework is presented in Figure 4. The analytical evaluation of a situation is as follows: dangerous floods seem very likely when the water level rises, as a drop in the measurements might indicate a mitigation of the situation. Clusters where a constant rise of the level y is observed represent a severe potential danger.

Let $T = \{t \in \mathbb{N}\}$ be a set that represents the number of time points where the measurements of the dataset were made. The time points where the level is rising can be described as:

$$T_{rising} = \{t \in T | y_t > y_{t-1}\} \tag{1}$$

Furthermore, the rising level is usually only dangerous after overcoming a certain level of interest β, which is specific to each catchment. The measurements over this lowest level of interest can be defined as

$$T_{relevant} = \{t \in T_{rising} | y_t > \beta\} \tag{2}$$

The time point where relevant measurements were taken can be separated into three sets

$$T_{relevant} = T_{ok} \cup \ T_{over} \cup T_{under} \tag{3}$$

Since the exact value is not needed in the application scenario, a certain level of tolerance b is introduced.

$$T_{ok} \quad = \{t \in T_{relevant} | \ |y_{pred} - y_{mes}| \leq b\} \tag{4}$$

Describes the time points where forecasted values are acceptable and can be considered as correct.

$$T_{over} \quad = \{t \in T_{relevant} | y_{pred} - y_{mes} > b\} \tag{5}$$

Are time points of overestimation of the model which could cause a potential false alarm.

$$T_{under} = \{t \in T_{relevant} | y_{pred} - y_{mes} < b\} \tag{6}$$

Are time points of underestimation of the model where a potential flood alert could have been overseen. These points are more critical than overestimation since the consequences of a false alert are less critical than the consequences of an overseen flood event. The event-focused evaluation framework was done by the definition of $\boldsymbol{\beta} = \mathbf{40}\ [\mathbf{cm}]$ as level where the dangerous flood can appear, and the acceptable variance of the prediction is $\boldsymbol{b} = \mathbf{10}\ [\mathbf{cm}]$. Both values have been consolidated with the safety concept of the city of Goslar.

These values can be interpreted accumulated as the number of time points where the model forecasted correct values or under- or overestimated the values during a flood event. Also, the interpretation of potential annual or relative right and false predictions can be made. This is especially useful when comparing models on datasets with different sizes.

The relative metrics are based on the amount of all events:

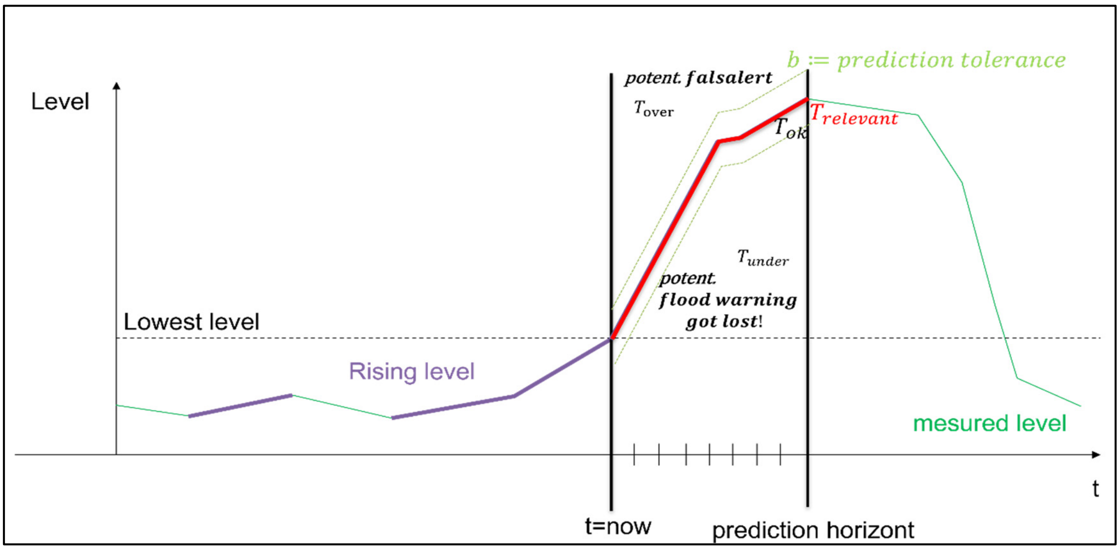

Figure 4: Schematic visualisation of the event-focused framework.

$$T_{all} = |T_{ok}| + |T_{under}| + |T_{over}| + |T_{not\ relevant}| \tag{7}$$

$$T_{ok\_relative} = \frac{|T_{ok}|}{T_{all}} \tag{8}$$

$$T_{over\_relative} = \frac{|T_{over}|}{T_{all}} \tag{9}$$

$$T_{under\_relative} = \frac{|T_{under}|}{T_{all}} \tag{10}$$

The annual comparison metrics have as a basis the number of years in which the relevant events were observed.

$$years\ observed = \frac{ammount\ observed\ events}{24 \times 4 \times 365} \tag{11}$$

$$T_{ok\_anual} = \frac{|T_{ok}|}{years\_observed} \tag{12}$$

$$T_{over\_anual} = \frac{|T_{over}|}{years\_observed} \tag{13}$$

$$T_{under\_anual} = \frac{|T_{under}|}{years\_observed} \tag{14}$$

While this measure gives a good comparative overview of the performance of different models in the predictive task, an interoperable metric related to the actual probability of missing dangerous events is still missing. For the example, a value of $T_{under\_anual} = 12$ can be understand a mean of 12 potential flood events per year, that would not be predicted correctly by the model. But there is no information on how cluttered this missed floods are. It is possible that these 12 events are spread out evenly across this year, meaning that only a single prediction for only a single 15 min interval is wrong every month. This would be a neglectable error, because all other prediction around this error would be correct and correctly implying an incoming flood, thus only reducing the warning time by 15 minutes. In the other extreme these 12 events could indeed be aligned in a single chain of errors hiding the flood for 3 hours. Also, the mean over the duration of observed years may have a high variance, with some years aggregating huge singe blind spots.

To tackle this issue, we added the statistic of chains of underestimated levels (events in T_{under}) as an additional metric. A chain in this context is defined as a subsequence of model predictions out of the ordered set of all model predictions in which all elements are within T_{under}. Intuitively speaking, how often the model underestimated a potential flood event in a row. If a chain is broken by a correct prediction, the parts are counted as different chains.

As a metric, we record the length of all chains longer than a single element, and the length of the longest chain, indicating the longest “blind spot” that the model would have in the context of a warning system.

5.2 Overall Metrics

To observe the performance of the model in all regions, outside and during the extreme event, the following overall metrics were adapted and applied (Krause et al., 2005):

r: Bravais Pearson Correlation Coefficient (BP), where one means that there is a perfect correlation between the observed values O and the predicted P, and zero when no correlation could be found. The correlation coefficient could be used as an additional indicator, but this coefficient is unsuitable for making judgments about the size of the error.

$$r = \frac{\sum_{i=1}^{n}(O_i - \bar{O})(P_i - \bar{P})}{\sqrt{\sum_{i=1}^{n}(O_i - \bar{O})^2}\sqrt{\sum_{i=1}^{n}(P_i - \bar{P})^2}} \tag{15}$$

E : Nash–Sutcliffe Efficiency (NSE) has, according to Krause et al., low sensitivity to systematic errors in lower regions and high systematic errors in peaks of prediction.

$$E = 1 - \frac{\sum_{i=1}^{n}(O_i - P_i)^2}{\sum_{i=1}^{n}(O_i - \bar{O})^2} \tag{16}$$

$$E = \begin{cases} 1 & : \quad \text{total fit} \\ -\infty & : \quad \text{no fit} \\ E < 0 & : \text{worse than average} \end{cases} \tag{17}$$

With the range $E \in [1: -\infty)$ it can be interpreted as follows:

d: Index of Agreement (IoA) faces the same tendency to overrate errors in peaks and underrate errors in lower regions.

$$d = 1 - \frac{\sum_{i=1}^{n}(O_i - P_i)^2}{\sum_{i=1}^{n}(|P_i - \bar{O}| + |P_i - \bar{O}|)^2} \tag{18}$$

With the range $d \in [1: 0\,]$, the interpretation of the model is as follows: $d = \begin{cases} 1\text{: total fit} \\ 0\text{: no fit} \end{cases}$

E_{mod}: Modified Nash–Sutcliffe Efficiency and d_{mod} modified Index of Agreement were alternated to be more sensitive in lower regions when the modification value J is smaller than two. In order to focus on peaks, the factor J should be alternated to values higher than 2. In this work, mainly the value $J = 3$ was used.

$$E_{mod} = 1 - \frac{\sum_{i=1}^{n}|O_i - P_i|^J}{\sum_{i=1}^{n}|O_i - \bar{O}|^J} \tag{19}$$

$$d_{mod} = 1 - \frac{\sum_{i=1}^{n}|O_i - P_i|^J}{\sum_{i=1}^{n}(|P_i - \bar{O}| + |P_i - \bar{O}|)^J} \tag{20}$$

Because the event-focused framework is mainly focused on rare, extreme events and the discussed overall metrics are adjusted to observe prediction errors in peaks, the systematic errors in lower regions could rise and give the observer overall wrong predictions. This could damage the reputation of the prediction model so that emergency services would only trust the values in higher regions where the model would give better results. To compare the overall prediction in lower regions, the modified Nash–Sutcliffe Efficiency and modified Index of Agreement with $J < 2$ should be used or as suggested, relative derivation of both these metrics.

The overall framework shows in all metrics a perfect fit. Meanwhile, all metrics show a poor result in absolute negative correlation (Figure 5).

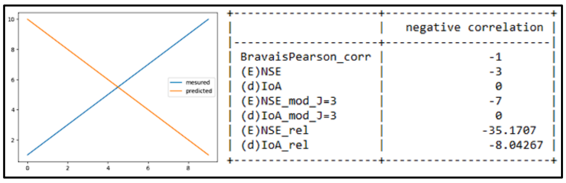

```
+----------------------+----------------------+
|                      | negative correlation |
|----------------------+----------------------|
| BravaisPearson_corr  |                   -1 |
| (E)NSE               |                   -3 |
| (d)IoA               |                    0 |
| (E)NSE_mod_J=3       |                   -7 |
| (d)IoA_mod_J=3       |                    0 |
| (E)NSE_rel           |             -35.1707 |
| (d)IoA_rel           |             -8.04267 |
+----------------------+----------------------+
```

Figure 5: Negative linear correlation.

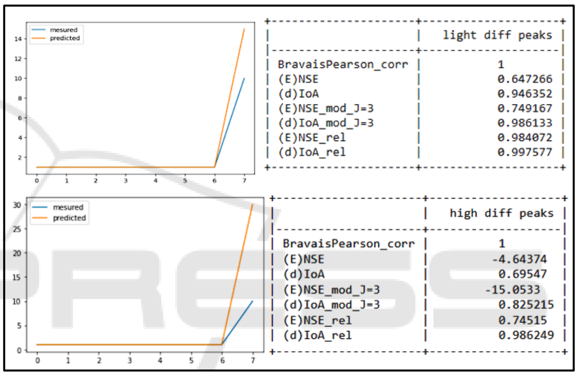

```
+----------------------+-------------------+
|                      |  light diff peaks |
|----------------------+-------------------|
| BravaisPearson_corr  |         1         |
| (E)NSE               |          0.647266 |
| (d)IoA               |          0.946352 |
| (E)NSE_mod_J=3       |          0.749167 |
| (d)IoA_mod_J=3       |          0.986133 |
| (E)NSE_rel           |          0.984072 |
| (d)IoA_rel           |          0.997577 |
+----------------------+-------------------+

+----------------------+------------------+
|                      |  high diff peaks |
|----------------------+------------------|
| BravaisPearson_corr  |         1        |
| (E)NSE               |       -4.64374   |
| (d)IoA               |        0.69547   |
| (E)NSE_mod_J=3       |      -15.0533    |
| (d)IoA_mod_J=3       |        0.825215  |
| (E)NSE_rel           |        0.74515   |
| (d)IoA_rel           |        0.986249  |
+----------------------+------------------+
```

Figure 6: Evaluation with the high and low differences in peak.

$$E_{rel} = 1 - \frac{\sum_{i=1}^{n}\left(\frac{O_i - P_i}{O_i}\right)^2}{\sum_{i=1}^{n}\left(\frac{O_i - \bar{O}}{\bar{O}}\right)^2} \tag{21}$$

$$d_{rel} = 1 - \frac{\sum_{i=1}^{n}\frac{(O_i - P_i)^2}{O_i}}{\sum_{i=1}^{n}\left(\frac{|P_i - \bar{O}| + |P_i - \bar{O}|}{\bar{O}}\right)^2} \tag{22}$$

In this framework, the relative metrics were chosen to observe lower regions since they have shown less sensitivity to small error changes.

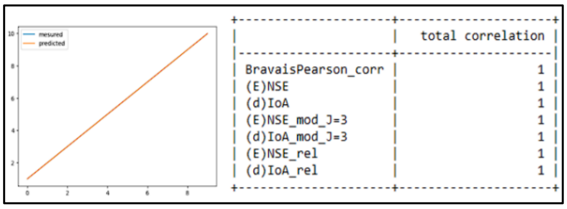

```
+----------------------+-------------------+
|                      | total correlation |
|----------------------+-------------------|
| BravaisPearson_corr  |                 1 |
| (E)NSE               |                 1 |
| (d)IoA               |                 1 |
| (E)NSE_mod_J=3       |                 1 |
| (d)IoA_mod_J=3       |                 1 |
| (E)NSE_rel           |                 1 |
| (d)IoA_rel           |                 1 |
+----------------------+-------------------+
```

Figure 7: Total linear correlation.

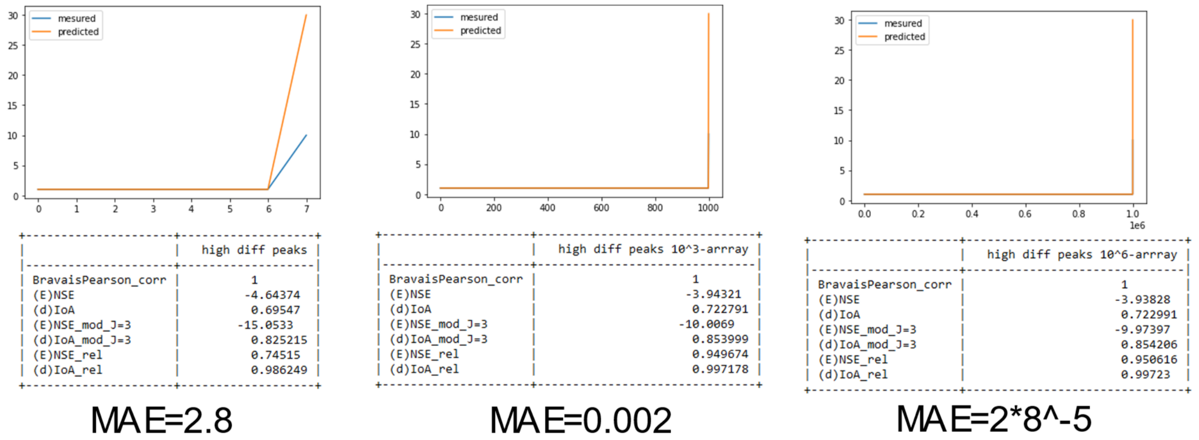

```
+------------------------+------------------------+
|                        |   high diff peaks      |
|------------------------+------------------------|
| BravaisPearson_corr    |          1             |
| (E)NSE                 |         -4.64374       |
| (d)IoA                 |          0.69547       |
| (E)NSE_mod_J=3         |        -15.0533        |
| (d)IoA_mod_J=3         |          0.825215      |
| (E)NSE_rel             |          0.74515       |
| (d)IoA_rel             |          0.986249      |
+------------------------+------------------------+
```

MAE=2.8

```
+------------------------+------------------------------+
|                        |   high diff peaks 10^3-arrray |
|------------------------+------------------------------|
| BravaisPearson_corr    |                      1        |
| (E)NSE                 |                     -3.94321  |
| (d)IoA                 |                      0.722791 |
| (E)NSE_mod_J=3         |                    -10.0069   |
| (d)IoA_mod_J=3         |                      0.853999 |
| (E)NSE_rel             |                      0.949674 |
| (d)IoA_rel             |                      0.997178 |
+------------------------+------------------------------+
```

MAE=0.002

```
+------------------------+------------------------------+
|                        |   high diff peaks 10^6-arrray |
|------------------------+------------------------------|
| BravaisPearson_corr    |                      1        |
| (E)NSE                 |                     -3.93828  |
| (d)IoA                 |                      0.722991 |
| (E)NSE_mod_J=3         |                     -9.97397  |
| (d)IoA_mod_J=3         |                      0.854206 |
| (E)NSE_rel             |                      0.950616 |
| (d)IoA_rel             |                      0.99723  |
+------------------------+------------------------------+
```

MAE=2*8^-5

Figure 8: Rising number of compared values.

To observe the behaviour of the overall metrics, different situations were modelled. In the first example, the observed values equal the measured O = P (Figure 7).

Two situations are modelled to observe the effect of error during peak, where all measured and predicted values are equal but one (Figure 6). In the first situation, the last value's absolute error is 5; in the second situation, the error of the peak is 20. The metrics clearly show that NSA and IoA are sensitive to the peak in the first situation and show the error change in the peak in the second situation. The modified NSA and IoA show similar results, and the relative NSA and IoA show that model performs well in lower regions. In all modified, relative and original metrics, IoA shows more stability, whereas NSA seems to be more sensitive.

The overall metrics generally show minimal sensitivity to the growing number of predicted values compared to the error. Unlike average-based metrics, the error did not approach zero, even with very high data. To observe the stability of the metric due to the growing number of measurements, the situation with an absolute error of 20 in the peak was alternated by growing from 8 to 10^3 and 10^6 measurements (Figure 8). The original and modified metrics could sense the error in the peak even when the model is improving due to the growing number of correct predicted values in the lower region. For the lower region, the relative metrics show a good performance of the estimated values and are improving with the growing number of equal measurements. Also remarkable is the stability of all alternations of IoA in these situations. In all these situations the BP coefficient is failing to show any changes due to a perfect correlation. Meanwhile, the Mean Absolute Error (MAE) shows clearly how a relatively significant error in a small dataset could lose importance with the growing size of the data.

6 REFERENCE MODELS

The criteria for a successful prevention of more significant damages from the sudden flood event in Goslar requires a prediction of the flood at least two hours in advance. Furthermore, rescue task forces could improve their actions with the larger forecast horizon. The results show that the forecast of 4 hours in the observed catchment is possible. Therefore, three models were generated with 2, 3 and 4 hours of the forecast horizon. For all 3-time horizons two architectures were tested; a simple LSTM-ANN with 32 neurons in each of four layers and a residual LSTM-ANN with 8 residual blocks and 6 neurons in each layer. All models take as input a series of 32 last observed values from each sensor, presented in Section 3, except from the data from Sennhuette and gives back a forecast of the value of data stream Sennhuette in 8, 12 or 16 future data points (2, 3 or 4 hours).Additional features were extracted to improve the model performance. The 2- hours model includes the gradient of the input of Sennhuette of one timestep (in the past). In 3- and 4-hour models, a gradient of 192 timesteps (in the past) for Sennhuette and the area under the curve for each of the two rainfalls were also calculated for the past 96 timesteps.

In the tests, the residual LSTM neural network outperformed the regular LSTM and the MLP of different architecture in forecasting the values during the extreme, unseen event. This might be explained by the capability of the residual ANN architectures to bypass input to the over layers. Meanwhile, in the regular ANN, the information is passed from the previous layer to the following. The residual neural network gives to one hidden layer the information that was generated by its direct predecessor and the information from one of the predecessors or even from the input layer. This reduces the risk of overfitting, where neuronal connections that seem to be unimportant are assigned lower weights and important new information is ignored.

The validation split of the training data was done with a pre-defined function of Keras-TensorFlow API with 20%. The training was done for a maximum of 30 epochs with the possibility of early stopping and a batch size of 265. The data was scaled using the method StandardScaler, from the library sklearn.

7 RESULTS

As mentioned before, the evaluation framework should be applied in two stages: the analysis of the defined rare–extreme event via the event-focused evaluation framework and the model's overall performance in lower and upper regions of the prediction via the overall metrics framework. Therefore, in the next two chapters, an evaluation of the residual LSTM-ANN is discussed and the comparison with the performance of the simple LSTM-ANN is done.

Table 2: Event focused evaluation of the LSTM-residual ANN.

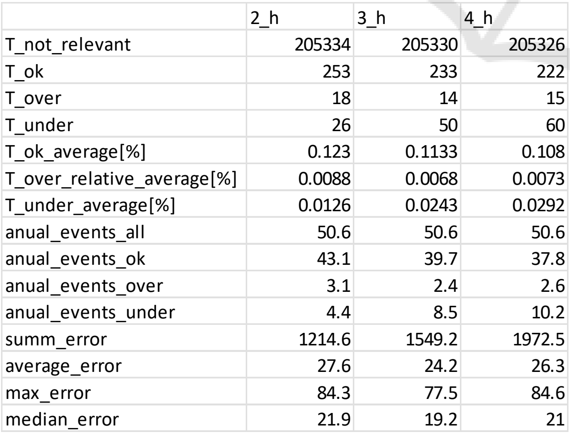

	2_h	3_h	4_h
T_not_relevant	205334	205330	205326
T_ok	253	233	222
T_over	18	14	15
T_under	26	50	60
T_ok_average[%]	0.123	0.1133	0.108
T_over_relative_average[%]	0.0088	0.0068	0.0073
T_under_average[%]	0.0126	0.0243	0.0292
anual_events_all	50.6	50.6	50.6
anual_events_ok	43.1	39.7	37.8
anual_events_over	3.1	2.4	2.6
anual_events_under	4.4	8.5	10.2
summ_error	1214.6	1549.2	1972.5
average_error	27.6	24.2	26.3
max_error	84.3	77.5	84.6
median_error	21.9	19.2	21

7.1 Evaluation Residual LSTM

In Table 2 it can be observed that the count of the timesteps where measurements are considered irrelevant have a difference of 4. This can be explained by the reshaping of the dataset. Since one hour is precisely four times 15 minutes, four data points are cut off for each prediction hour. Since the relevant points are not at the beginning nor at the end of the dataset, they are not affected. The amount of $T_{relevant} = \{T_{ok}, T_{over}, T_{under}\} = 297$ in all three models shows the robust detection of the extreme event, regardless of the used model. Nonetheless, the distribution of the absolute amount of $T_{ok}, T_{over}, T_{under}$ is different. While the number of overrated events is not showing a clear trend and are in the range of 14-18, the range of underrated events shows a clear and robust trend from 26 underrated events in the 2 hours prediction to almost double, 50 in the 3 hours prediction and 60 for the 4 hours prediction. Proportionally, the number of right-guessed events (T_{ok}) is sinking with each additional forecasted hour. This trend can be observed in absolute and in relative numbers. The most dangerous, underrated annual events proportionately grow from 4.4 to 10.2 times. This means that, annually, the model would wrongly predict about four events in two-hour prediction, around nine events for three and ten events in a four-hour prediction.

Table 3: Residual-LSTM overall metric evaluation.

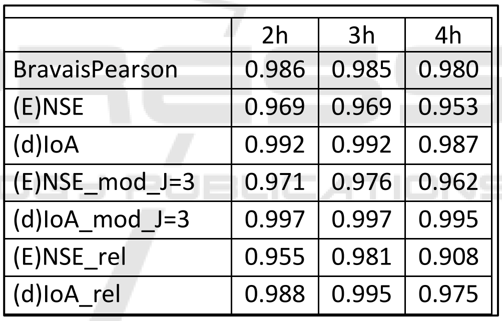

	2h	3h	4h
BravaisPearson	0.986	0.985	0.980
(E)NSE	0.969	0.969	0.953
(d)IoA	0.992	0.992	0.987
(E)NSE_mod_J=3	0.971	0.976	0.962
(d)IoA_mod_J=3	0.997	0.997	0.995
(E)NSE_rel	0.955	0.981	0.908
(d)IoA_rel	0.988	0.995	0.975

The sum of errors made during the event shows a similar trend of growing with the prediction horizon. The overall metric evaluation in Table 2 does not show a clear trend between the two- and three-hours model. Meanwhile, the original overall metrics show a better performance of the two-hours model and the modified NSE and IoE show the superior prediction of the three-hours model in higher regions. The relative metrics also show better performance in the lower regions. All metrics show the 4 hours model performance as the worst.

It can be said that the overall performance of all three models is very close to each other. The slight differences should be noticed and observed. The event-focused framework, which considers the extreme and dangerous event, says clearly that the model with a smaller horizon is outperforming the model with a wider horizon and seems more reliable in dangerous situations.

Table 4: Simple architecture LSTM-neuronal network event-focused framework.

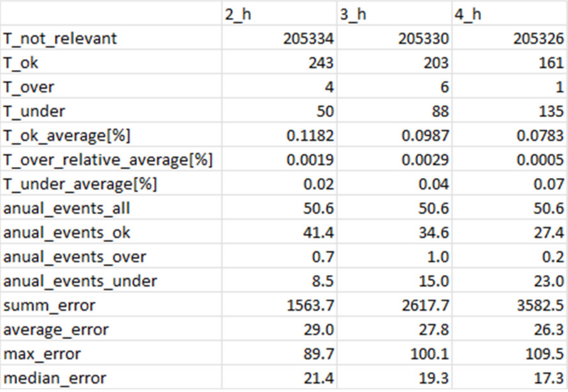

	2_h	3_h	4_h
T_not_relevant	205334	205330	205326
T_ok	243	203	161
T_over	4	6	1
T_under	50	88	135
T_ok_average[%]	0.1182	0.0987	0.0783
T_over_relative_average[%]	0.0019	0.0029	0.0005
T_under_average[%]	0.02	0.04	0.07
anual_events_all	50.6	50.6	50.6
anual_events_ok	41.4	34.6	27.4
anual_events_over	0.7	1.0	0.2
anual_events_under	8.5	15.0	23.0
summ_error	1563.7	2617.7	3582.5
average_error	29.0	27.8	26.3
max_error	89.7	100.1	109.5
median_error	21.4	19.3	17.3

7.2 Evaluation of Simple LSTM

As mentioned before, the initial goal of the evaluation framework is not only to investigate the performance of one kind of architecture but to evaluate two or more architectures in comparison to each other. Therefore, a simple LSTM-ANN was prepared.

In Table 4 one can observe the apparent change of the distribution of the time points where measurements were overrated and underrated. Meanwhile, the residual LSTM-ANN also has a high number of overrated measurements during the event.

Table 5: Simple-LSTM overall metric evaluation.

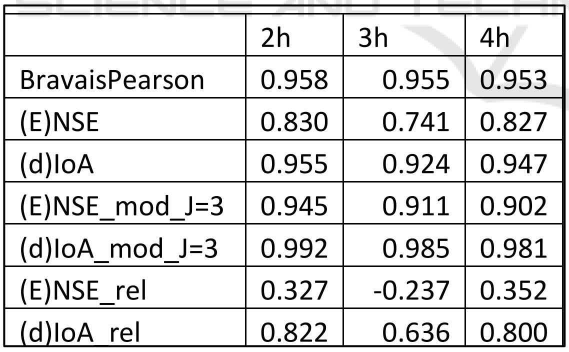

	2h	3h	4h
BravaisPearson	0.958	0.955	0.953
(E)NSE	0.830	0.741	0.827
(d)IoA	0.955	0.924	0.947
(E)NSE_mod_J=3	0.945	0.911	0.902
(d)IoA_mod_J=3	0.992	0.985	0.981
(E)NSE_rel	0.327	-0.237	0.352
(d)IoA_rel	0.822	0.636	0.800

The simple architecture of LSTM shows a trend towards underrating more overrating a measurement. With 50, 88 or 135 it has almost doubled the amount of the underrated measurements. Furthermore, it reduces the number of right-guessed forecasts. This trend can be observed also in relative evaluation, meanwhile the average error or median fails to represent the difference. However, the overall framework analysis in Table 5 shows that this architecture has generally worse performance in upper regions (NSE, IoA and modified NSE and IoA) and awful performance in lower regions, according to relative NSE and IoE. The interpretation of the number is that the model makes a systematic error in lower regions. Though the performance in higher regions is rising, it has more errors than the residual LSTM-ANN. This observation can be confirmed with the event-focused evaluation in Table 4. The performance difference during the extreme event can be qualitatively observed in Figure 11 and Figure 12. The observation of the overall performance of both models can be done in Figure 10 and Figure 9. Meanwhile, the residual ANN-model prediction visually covers the measured level, the simple LSTM ANN-model shows systematical overprediction in the lower region and high underrating during extreme events.

The Table 6 gives a comprehensive overview of the distribution of error-chains among the models and for the different prediction horizons. The last raw of the table shows the average length of all chains. The residual LSTM-ANN produces consistently slightly shorter longest chains than the simple LSTM-ANN (9 versus 10) and also sorter chains on average (2.3:3.9; 4.1:8.1; 5.4:11).

Table 6: Distribution of chain length among models and prediction horizons.

	2h		3h		4h	
length	simple	residual	simple	residual	simple	residual
2	5	3	9	5	10	8
3	3	0	5	0	3	2
4	0	0	3	1	5	1
5	0	0	1	0	0	0
6	1	1	1	1	2	1
7	0	0	0	0	1	0
8	0	0	1	1	1	1
9	0	1	0	1	1	1
10	1	0	1	0	1	0
Average length	3,9	2,3	8,2	4,1	11	5,4

8 CONCLUSIONS

In this article, we presented a benchmark for machine learning-based forecasting models. One crucial part of the benchmark is the real-world data from the settlement Goslar in Germany that were collected from Harzwasserwerke GmbH for 14 years.

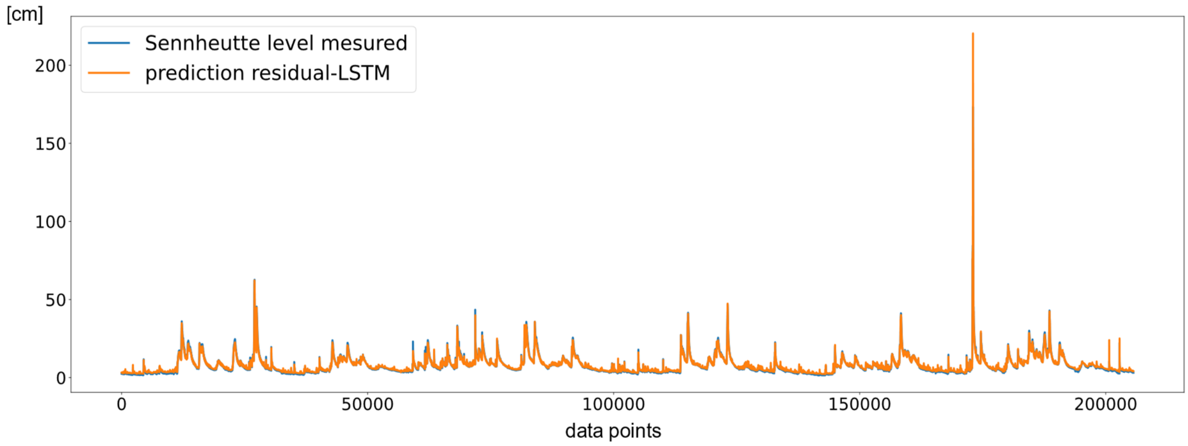

Figure 9: Overall prediction line of residual LSTM-ANN.

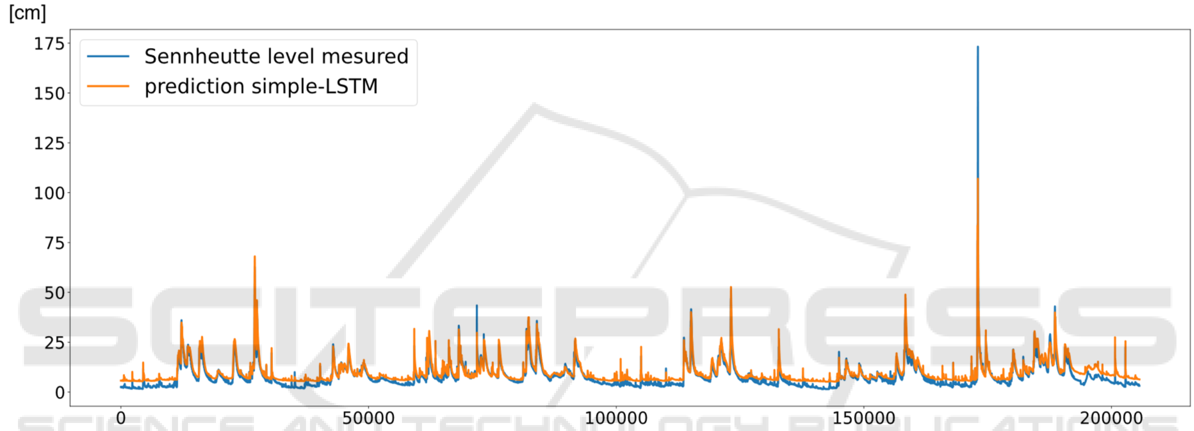

Figure 10: Overall prediction line of simple LSTM-ANN.

We discussed the problem that ANN are facing during the prediction of unseen, extreme events like floods caused by sudden rain as it happened in the year 2017 in Goslar. The presented results of the residual LSTM-ANN could outperform the regular LSTM-ANN during the regular operation and the extreme event. The discussed and presented framework that consists of an overall evaluation framework and event-focused evaluation framework could prove the improvement of the used model. The robust evaluation allows further evaluation of risks for the city of Goslar's safety concepts. The presented models are also a part of the actual real-time observation system in the settlement.

Nevertheless, the benchmark gives a consolidated and substantial challenge for machine-learning-based models that should be applied to rare, extreme events. The framework's flexibility also allows the evaluation on settlements with other geological conditions.

The consolidation of the benchmark allows for improvement in the methods of forecasting and evaluating the constantly evolving research of machine learning algorithms in the area of hydrogeology.

ACKNOWLEDGEMENTS

At this point, thanks to all the people who supported this work during the execution of the project and preparation of this paper. Our special thanks goes to the Harzwasserwerke GmbH for providing the data from the measuring stations in Goslar and Bad Harzburg and to the city of Goslar for great collaboration and providing the local geohydrological domain knowledge. Also our thanks to Niedersächsischer Landesbetrieb für Wasserwirtschaft, Küsten- und Naturschutz (NLWKN) and Niedersächsisches Ministerium für Umwelt, Energie und Klimaschutz for funding of the project “Goslar - KI Hochwasserfrühwarnsystem”.

REFERENCES

Alfieri, L., Bisselink, B., Dottori, F., Naumann, G., Roo, A. de, Salamon, P., Wyser, K., and Feyen, L. (2017). “Global projections of river flood risk in a warmer world,” Earth's Future. Vol. 5, No. 2: pp. 171–182.

Allamano, P., Claps, P., and Laio, F. (2009). “Global warming increases flood risk in mountainous areas,” Geophysical Research Letters. Vol. 36, No. 24.

Danso-Amoako, E., Scholz, M., Kalimeris, N., Yang, Q., and Shao, J. (2012). “Predicting dam failure risk for sustainable flood retention basins: A generic case study for the wider Greater Manchester area,” Computers, Environment and Urban Systems. Vol. 36, No. 5: pp. 423–433.

Dtissibe, F. Y., Ari, A. A. A., Titouna, C., Thiare, O., and Gueroui, A. M. (2020). “Flood forecasting based on an artificial neural network scheme,” Natural Hazards. Vol. 104, No. 2: pp. 1211–1237.

Goymann, P., Herrling, D., and Rausch, A. (2019). “Flood Prediction through Artificial Neural Networks: A case study in Goslar, Lower Saxony,” in ADAPTIVE 2019: The Eleventh International Conference on Adaptive and Self-Adaptive Systems and Applications : May 5-9, 2019, Venice, Italy, N. Abchiche-Mimouni (ed.), Wilmington, DE, USA: IARIA, pp. 56–62.

Hettiarachchi, P., Hall, M. J., and Minns, A. W. (2005). “The extrapolation of artificial neural networks for the modelling of rainfall—runoff relationships,” Journal of Hydroinformatics. Vol. 7, No. 4: pp. 291–296.

Jimeno-Sáez, P., Senent-Aparicio, J., Pérez-Sánchez, J., Pulido-Velazquez, D., and Cecilia, J. (2017). “Estimation of Instantaneous Peak Flow Using Machine-Learning Models and Empirical Formula in Peninsular Spain,” Water. Vol. 9, No. 5: p. 347.

Kim, S., Matsumi, Y., Pan, S., and Mase, H. (2016). “A real-time forecast model using artificial neural network for after-runner storm surges on the Tottori coast, Japan,” Ocean Engineering. Vol. 122, pp. 44–53.

Krause, P., Boyle, D. P., and Bäse, F. (2005). “Comparison of different efficiency criteria for hydrological model assessment,” Advances in Geosciences. Vol. 5, pp. 89–97.

Minns, A. W., and Hall, M. J. (1996). “Artificial neural networks as rainfall-runoff models,” Hydrological Sciences Journal. Vol. 41, No. 3: pp. 399–417.

Mosavi, A., Ozturk, P., and Chau, K. (2018). “Flood Prediction Using Machine Learning Models: Literature Review,” Water. Vol. 10, No. 11: p. 1536.

Mulualem, G. M., and Liou, Y.-A. (2020). “Application of Artificial Neural Networks in Forecasting a Standardized Precipitation Evapotranspiration Index for the Upper Blue Nile Basin,” Water. Vol. 12, No. 3: p. 643.

Pektas, A. O., and Cigizoglu, H. K. (2017). “Investigating the extrapolation performance of neural network models in suspended sediment data,” Hydrological Sciences Journal. Vol. 62, No. 10: pp. 1694–1703.

Riad, S., Mania, J., Bouchaou, L., and Najjar, Y. (2004). “Rainfall-runoff model usingan artificial neural network approach,” Mathematical and Computer Modelling. Vol. 40, 7-8: pp. 839–846.

Shamseldin, A. Y. (2010). “Artificial neural network model for river flow forecasting in a developing country,” Journal of Hydroinformatics. Vol. 12, No. 1: pp. 22–35.

Xu, K., Zhang, M., Li, J., Du S, S., Kawarabayashi, K., and Jegelka, S. (2020). How Neural Networks Extrapolate: From Feedforward to Graph Neural Networks.